



Sampling density and spatial analysis: a methodological pXRF study of the geochemistry of a Viking-Age house in Ribe, Denmark

Pernille L. K. Trant^{1,2} · Søren M. Kristiansen^{1,2} · Anders V. Christiansen¹ · Barbora Wouters^{2,3,4} · Søren M. Sindbæk²

Received: 17 February 2020 / Accepted: 23 November 2020
© Springer-Verlag GmbH Germany, part of Springer Nature 2021

Abstract

This study explores the significance of spatial sampling resolution on portable X-ray fluorescence (pXRF) analysis of an archaeological settlement site with favorable preservation conditions and clearly defined stratigraphic contexts as a benchmark study to interpret geochemical mapping of anthropogenic elemental markers. We present geochemical elemental mapping of a Viking-Age house floor in Denmark based on an unprecedented sampling density of a 0.25-m grid. In order to establish a fast, cost-efficient, comparable approach of how different sizes of data resolution affect the spatial elemental patterns, the data is analysed using three different grid sizes: 0.25 m × 0.25 m, 0.5 m × 0.5 m, and 1.0 m × 1.0 m. We analysed each grid size with selected anthropogenic markers (CaO, Cu, P₂O₅, and Sr) using ordinary kriging. The CaO, P₂O₅, and Sr patterns display a strong inter-correlation between data points up to a distance of 1–1.5 m from one another. At the highest resolution (0.25-m grid), all of the elements display a high degree of detail in the variation of the elements across the indoor surface with low standard deviations. Hence, the precise position of hot and coldspots, and spread of bounded concentration zones, is easily recognized in the maps. With the low resolution (1.0-m grid), the borders between high and low concentrations become more blurred and the indications of smaller hotspots (possible activity areas) are completely lost. Especially, Cu displays a high degree of clustering, which the high-resolution sampling could best reveal. This benchmark study shows that it is realistic to perform large-scale geochemical surveys of archaeological settlements using pXRF spectrometry in a standard archaeological excavation context, but also that sampling distances of 0.5 m × 0.5 m or finer are best suited to in indoor contexts.

Keywords Viking Age · Urbanisation · Indoor activity · Sampling design · Geochemistry · Anthropogenic elemental markers

Introduction

The organization and use of space in domestic contexts has become a central topic in archaeological investigations as a way of exploring activities and organization of families and households in past societies (e.g. Cook et al. 2014; Crabtree et al. 2017; Croix 2015; Macphail et al. 2016; Milek 2012; Milek et al. 2014; Rondelli et al. 2014; Smith et al. 2001;

Sulas et al. 2019). Recent studies have approached these issues through the spatial distribution of artefacts or ecofacts, and increasingly also geoarchaeological methods including micromorphology (e.g. Barrett et al. 2007; Milek 2012; Milek and Roberts 2013; Milek and French 2007; Save et al. 2020; Skre 2007). Activities can also be recognized by anthropogenic elemental signatures in soil geochemical maps (Woodruff et al. 2009). Case studies have shown conclusive evidence of the correlation between elemental signatures and the use of domestic space in ethnographic contexts (e.g. Dore and Varela 2010; Rondelli et al. 2014). Much further work is nevertheless needed to understand how geochemical signatures are captured, combined, and preserved in archaeological contexts.

On in situ surfaces, even ancient human activity will leave chemical traces or disturbances as either an enrichment or depletion of the geochemical signature in the substrate, as long as the floor is not entirely impermeable (Mikołajczyk and Milek 2016; Pîrnău et al. 2020; Save et al. 2020; Sulas et al.

✉ Pernille L. K. Trant
pernille@trant.dk

¹ Department of Geoscience, Aarhus University, Aarhus, Denmark

² Centre for Urban Network Evolutions, Aarhus University, Aarhus, Denmark

³ Research Foundation Flanders – FWO, Brussels, Belgium

⁴ Maritime Cultures Research Institute, Vrije Universiteit Brussel, Brussels, Belgium

2019). In this case, the geochemical signal will be recorded in the occupation deposits formed, and can thus be detected using different geochemical methods. Previous studies have applied different geochemical methods to measure fluctuations in element concentrations across a surface and presented the results as isopleth maps (e.g. Milek and Roberts 2013; Milek et al. 2014). However, as noted by Dore and Varela (2010) this approach has limitations regarding the interpretation of use of space and visualization of the geochemical data (Dore and Varela 2010). Thus, Dore and Varela (2010) suggested a new approach for spatial analysis of multivariate datasets using interpolation methods. This was applied with some modifications, to an outdoor area on a farmstead in Iceland by Mikołajczyk and Milek (2016), and revealed different activity areas providing information about the functional character and evolution of each area.

Traditionally, laboratory methods such as inductively coupled plasma atomic emission spectroscopy (ICP-AES) or mass spectroscopy (ICP-MS), loss on ignition (LOI), magnetic susceptibility, and X-ray fluorescence (XRF) have been used to study changes in elemental concentrations at archaeological sites (e.g. Cook et al. 2014; Linderholm 2007; Macphail et al. 2004; Milek and Roberts 2013; Milek et al. 2014; Sulas et al. 2019; Wilson et al. 2005, 2008). More recently, quicker and more cost-efficient methods that replace wet chemistry for the analysis of soil elements and permit large-scale routine soil mapping, such as portable X-ray fluorescence (pXRF), have been included in pedogenesis and geoarchaeological studies (e.g. Abrahams et al. 2010; Horák et al. 2018; Lubos et al. 2016; Mikołajczyk and Milek 2016; O'Rourke et al. 2016; Pîrnău et al. 2020; Save et al. 2020; Šmejda et al. 2018; Stockmann et al. 2016). As a result, this method has been recognized as an effective tool for soil analysis in studies of pedogenesis (Stockmann et al. 2016) and mapping of the use of space in archaeological contexts (Fleisher and Sulas 2015). Other handheld instruments, such as laser-induced breakdown spectroscopy (LIBS), magnetic susceptibility, and visible near- and mid-infrared spectroscopy (vis-NIRS and MIRS), are also developing fast in adjacent sciences (Nicolodelli et al. 2019; Zhao et al. 2019), and are promising tools for supporting on-site archaeological interpretation, either as stand-alone methods, in combination with pXRF, or together with geophysics (Cannell et al. 2018; Fleisher and Sulas 2015).

The application of fast methods such as pXRF also offers the opportunity to apply thorough spatial geostatistical analyses (e.g. Fleisher and Sulas 2015; Lubos et al. 2016; Pîrnău et al. 2020; Rondelli et al. 2014; Thompson et al. 2018). Geostatistical estimation and interpolation such as kriging, which includes spatial data variation, allows for detailed studies of correlation between parameters as well as the uncertainties introduced by interpolation to provide unbiased estimates with minimum variance (Oliver and Webster 2014). A

key part of kriging is modelling of the semivariogram, which is a measure for the spatial dependencies and structures arising from the underlying spatial variation held in the data. Kriging is then applied to predict values of a given soil parameter in unsampled locations using the semivariogram model (Entwistle et al. 2007; Webster and Oliver 1990). Kriging is the most widely applied technique for geostatistical modelling of spatial contexts, and different kriging methods have different potential in predicting the spatial variability (Rondelli et al. 2014). The method is not yet widely applied to archaeological sites, but several studies have already demonstrated its potential (e.g. Cook et al. 2005; Entwistle et al. 2007; Haslam and Tibbett 2004; Wells et al. 2007; Wells 2010).

It is well known that the archaeological record includes traces of human activities in the sediments' elemental composition. However, there is a general lack of studies regarding the spatial resolution to which we can study small-scale variations in elemental concentrations across indoor areas. The methodology for investigating activity areas based on geochemistry has recently further been developed and established in work conducted by Dore and Varela (2010) and Mikołajczyk and Milek (2016). Some anthropogenic elements might only be correlated to one or two activities (e.g. Sulas et al. 2019), and as a result the corresponding elemental pattern can be limited in extent and, thus, might display a hotspot tendency. Here, a hotspot is considered to be a small collection of samples with concentrations much higher than the mean, i.e. Cu at > 50% mean in this study. Detection of such indoor hotspots needs to be evaluated in terms of its recognisability as a result of the sampling density, as human indoor activities leave behind different soil patterns compared to e.g. stabled animal husbandry (Macphail et al. 2004).

Our aim is to study the optimal sampling resolution based on pXRF elemental measurements on a site with relatively favorable indoor preservation conditions and clearly defined stratigraphic contexts as a benchmark study to understand geochemical investigations in less well-preserved settings. In doing so, this methodological study thus evaluates how different sampling densities (meaning different resolutions of sampling grids) affect the visualization of the spatial distribution of elements across an indoor surface, and how dense the sampling should be for the samples to be statistically correlated. An additional rationale is a cost-efficient application with an increased potential use in daily routine fieldwork in a context of developer-funded archaeology.

Materials and methods

Study area

The trading town or emporium Ribe (Fig. 1) emerged in the early 8th century as a part of the maritime trading network in

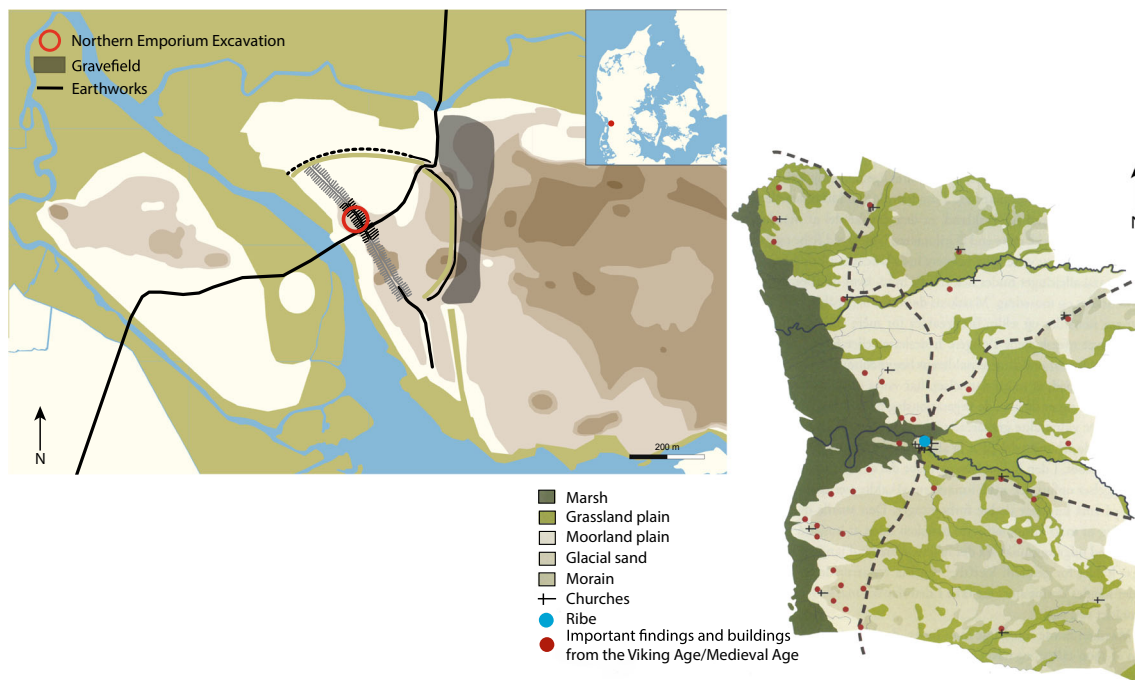


Fig. 1 Left: Reconstruction of the townscape of Ribe's emporium in the Viking Age. The red circle marks the approximate location of the Northern Emporium Excavation. The market site (from ca. 700 AD onwards) is represented by two rows of parallel plots on either side of a median street. The earthworks only appear after the middle of the ninth

century. The grave field to the east was mostly in use in the eighth and early ninth centuries. Graphics: Morten Søvsø and Louise Hilmar. Right: The geology of the southwestern part of Denmark with the location of Ribe and important findings from the Viking Age in the area. Modified after Feveile (2010)

the northern Wadden Sea (Croix 2015). By the end of the 8th century, it had grown into a dense, permanent settlement with two parallel rows of plots with wattle houses, divided by a narrow street and ditches in-between. Together with trading activities, the site housed a range of specialist crafts including copper-alloy metalworking (Croix 2015; Feveile 2006, 2012; Feveile and Jensen 2000; Jensen 1991).

Ribe is located approximately 5.5 km inland at a point where a dry, sandy Ice Age hill island meets the marshland of the Wadden Sea coast (Fig. 1). During the Viking Age, Ribe was accessible by ship from the Wadden Sea on the stream Ribe Å (Feveile 2010). The Viking-Age part of Ribe south of the stream is placed on a small outwash bank of glacial age (Mertz 1977) covered by aeolian sand deposited around 2000 BP (Dalsgaard 2005). The marshland west of the town provides grazing areas for livestock (Mertz 1977) and potentially clay as building materials.

During 2017 and 2018, the Northern Emporium Excavation Project conducted a full stratigraphic excavation of a central part of Viking-Age Ribe (Sindbæk 2018). The excavation was located at what is today known as "Posthustorvet" (the area between the Art Museum, Sct. Nikolaj Gade 10, and the former Post Office) in the centre of modern-day Ribe and close to earlier excavations (see

Feveile 2006; Sindbæk 2018). The excavation covered almost the full extent of one building plot (Plot 1), including ditches on both sides, the front part of the opposite plot (Plot 2), and the street separating both plots. On Plot 1, the excavation uncovered several clay layers belonging to different successive buildings and activity phases from the earliest stages of the settlement. The clay layers seem to reflect 'passive' floor layers (*sensu* Gé et al. 1993), constructed for the purpose of levelling and stability or the complete rebuilding of the houses on top of older structures. These clay floors, and the associated occupation deposits formed on top of them, can provide valuable information about the activities that took place inside houses at this early stage of urbanisation in Viking-Age Denmark.

The Northern Emporium excavation of Ribe applied an excavation strategy encompassing systematic 3D laser scanning, and intensive and large-scale micromorphological sampling as an integrated part of the excavation record (Croix et al. 2019). Similar high-definition excavation strategies are anticipated to be more widespread and an understanding of cost-efficiency in the targeted sampling of excavation units is increasingly important for archaeological field practices.

To test the application of high-resolution multi-proxy analyses for the use of urban spaces, we chose to target an

archaeologically interpreted indoor occupation deposit with thorough sampling for geochemistry along a dense grid. The subsequent excavation showed that most of the sampled layers belonged to the upper phase of the house designated as “K22”, but due to indistinctness in the stratigraphy, some limited areas contain remains from the lower phase of a younger house “K23” comprising a workshop for non-ferrous metal-working recognized during excavation (Fig. 2). Difficulties in separating different layers of clay arose from the sinking and deformation of the stratigraphy due to underlying features rich in organic matter. The sampled floor layers measure approximately 7×10 m, and are radiocarbon dated to the period c. 780–820 CE (Philippsen et al., in prep.).

The targeted occupation deposits (Figs. 2 and 3) occurred in the excavation as thin, dark-brown layers with a thickness varying from a few millimeters to a couple of cm directly overlying the clay floors. Table 1 includes the full description of recognized excavation units. On-site, two side aisles, a middle aisle, and two front rooms were distinguished according to differences in sediment colour and texture.

The main part of the targeted occupation deposits belong to house K22 phase c. K22c includes the following stratigraphic units: lowermost are the clay floors defining the outline of the house (excavation units A280–A283 and A285, see Fig. 2), a collapsed baking oven (i.a. A276) and activity, sand and ash layers (among others A262 and A263). Of these excavation units, only the occupation deposits A262 and A263, the hearth A273, and the baking oven A276 were sampled for geochemistry (Fig. 3).

At the time of sampling, K22c was disturbed by younger features from the lowermost phase of house K23 (excavation units A264 and A273). House K23 consists of a sequence of layers including among others its lowermost clay floors, a hearth, and two occupation deposits. From K23, only one of the occupation deposits (A264) and the hearth (A273) were included in the sampling.

In addition to the layers from within house K22c and K23, the sampling also covered an outdoor area (A266) south of the house interpreted as a shallow ditch or pathway, which contained large amounts of animal bones in a dark homogeneous matrix, as well as part of the road northeast of the house (A243) which was observed as dark sediment with a patch of light sand (A265, see Fig. 3).

Sampling and sample preparation

Undisturbed sediments from the two houses, K22c and K23 and adjacent shallow ditch, road, and back area, were bulk sampled across the entire surface along a $0.25\text{-m} \times 0.25\text{-m}$ grid (Fig. 3a). Due to post-depositional processes, the site was significantly sloping towards the side aisles and ditches. As a result, an artificial horizontal grid was projected onto the sloping surface using coordinates and a Trimble SX10 (DGPS) high-density 3D laser scanning total station. On every grid point, a skewer was placed to mark the intersections, and sub-cm precise, real-time coordinates of each sample in the grid were recorded. All sediment samples were taken up to a 10-cm radius around each grid point and care was taken not to include any underlying layers. Sampling bias was minimized

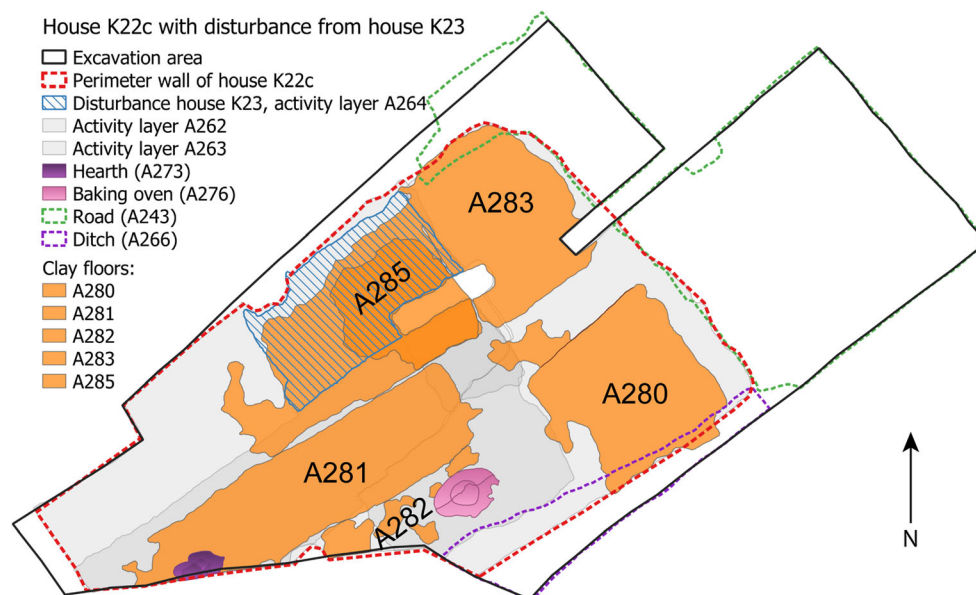


Fig. 2 House phase K22c with disturbance from house K23 (occupation deposit A264 and the sunken feature hearth A273). House phase K22c is defined by the clay floors A280–A283 and A285. The sampled

occupation deposits A262 and A263 that overlie the clay floors and the baking oven A276 are also shown. The shown house phase was radiocarbon dated to the period c. 780–820 CE

Table 1 Description of excavation units recognized on-site from house K22c and K23

Unit no.	Thickness	Description	Interpretation
A262	5–7 cm	Heterogeneous mixture of greyish brown sand rich in organic matter; and greenish clayey silt. Boundaries range from sharp to diffuse. Moderate to strong bioturbation. Inclusions of smaller flint gravel within the sand.	Activity deposit in K22 phase c
A263	3–5 cm	As A262	Activity deposit in house K22 phase c
A264		Lamination of predominantly orange-coloured sand; grey silty clay with temper of horizontally bedded organic matter and traces of organic bedding (woven grass or hay/straw); and charcoal-rich sand. Inclusions of large burnt clay and/or daub aggregates, glass slag, calcined bone (up to 5 cm), metal finds, and a metal-filled crucible. Wavy to somewhat diffuse boundaries.	Activity deposit in house K23
A273	5–10 cm	Homogeneous, orange-red, compacted clay with traces of burning and hardening at the very top.	Hearth in house K23
A276	10–12 cm	The bottom level consisted of greenish-yellow unburnt clay. In the middle was a distinct surface of yellow to orange clay with traces of burning. The top was represented by a 5-cm-thick layer yellow to orange clay with traces of burning and a lumpy, but still compact structure.	Remains of collapsed baking oven in house K22 phase c
A280	0–5 cm	Two thin, homogeneous, greenish-yellowish silty clay layers separated by a thin, dark-brown sand layer containing ash.	Part of clay floor in house K22 phase c
A281	0–5 cm	Porous, homogeneous red to orange silty clay of varying thickness, thinnest in the middle where the layer was almost worn away in some places.	Part of clay floor in house K22 phase c
A282	0–5 cm	A homogenous, only sporadically preserved, yellowish grey, thin, silty clay.	Part of clay floor in house K22 phase c
A283	0–5 cm	A lamination of several thin, homogeneous yellowish grey silty clay layers separated by thin dark-brown sand layers containing organic matter and ash.	Part of clay floor in house K22 phase c

by securing that all samples were collected by the same individuals during three days only. Each bulk soil sample weighed approximately 150 g and was numbered according to the grid. In total, 1059 bulk samples were collected.

All 1059 samples were air dried at low temperature (approximately 27 °C), gently powdered with a ceramic mortar and pestle and 2-mm dry sieved to remove any components > 2 mm. Finally, approximately 30 ml of each sample was representatively subsampled making sure all size fractions were included, ground using a Retsch RS200 to ensure homogeneity, and stored in medicine glasses.

Laboratory analyses

All 1059 soil samples were analysed in the laboratory using a standardized set-up and a Bruker S1 Titan 800 portable XRF scanner with an Rh anode tube and a maximum voltage of 50 kV/39 µA. The instrument works with a collimation standard of 5 mm and a five position motorized filter changer. For the analyses, the chosen application was the mining mode “GeoChem” with method “GeoChem General”, which includes full support for light elements through dual phase measurements. Preceding the main analysis, a reference sample with known elemental values was measured several times in order to choose the phase settings that gave the best replication with shortest exposure times. Based on this, the phase settings were selected to 30 s for both the first and second phase. The reference sample was

measured in between samples to account for possible drifting in the instrument. Each sample was analysed three times and the resulting mean of each element was used.

Samples were analysed for 38 different elements as standard. From these, four elements (calcium, copper, phosphorus, and strontium) were selected for further study. These elements were selected since they are already known as indicators of different indoor activities (Milek and Roberts 2013; Sulas et al. 2019). The rationale for selecting four elements only in this methodological study is that they cover the overall variations expected from both natural and anthropogenic sources (e.g. Sulas et al. 2019). First, phosphorus is found to be the best ethnographic and archaeological indicator in most geochemical studies and is associated with a variety of sources, such as foodstuffs in general, dung, marine foodstuffs, household waste, middens, and hearths (Mikołajczyk and Milek 2016; Milek and Roberts 2013; Sulas et al. 2017; Sulas et al. 2019). Next, copper is a tracer of metalworking but also household waste, middens, and hearths (Fleisher and Sulas 2015; Sulas et al. 2017, 2019). Calcium and strontium are potential indicators of the texture and the mineralogical assemblage associated with the variations in the parent soil materials in the local, naturally acidic soils, but in these purely anthropogenic deposits they should be regarded as anthropogenic markers for e.g. plant nutrients and bone (foodstuffs in general), wood ash, general household waste, middens, and hearth deposits (Cook et al. 2014; Fleisher and Sulas 2015; Mikołajczyk and Milek 2016; Milek and Roberts 2013; Sulas et al. 2017, 2019). The

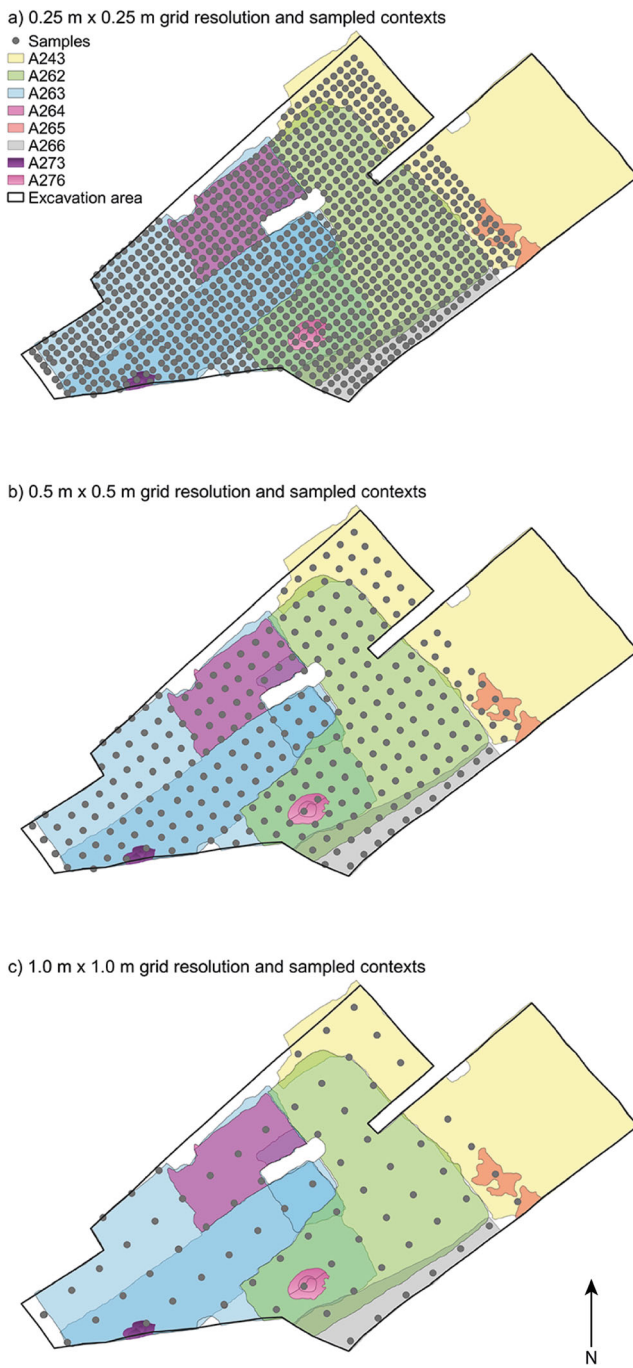


Fig. 3 Location of the three grids applied, **a** 0.25 m × 0.25 m, **b** 0.5 m × 0.5 m, and **c** 1.0 m × 1.0 m and all sampled excavation units. The sampled excavation units cover the occupation deposits (A262 and A263) and the baking oven (A276) from house phase K22c with disturbance from an occupation deposit (A264) and the sunken feature hearth (A273) from house K23. Part of the road (A243 and A265) and the southern ditch (A266) were also covered by the geochemistry sampling

archaeological interpretation of the full set of elements in our grid has to be based on a multi-scalar, multi-method approach and is thus not discussed here.

No natural reference material analyses are included in this paper. Since (a) the main aim is to discuss relative enrichment

patterns vs. sampling grid size, and (b) as the European GEMAS project data (Reimann et al. 2018) are derived from agricultural and from grassland soils, which in Denmark share the same intensive land use history for > 200 years with addition of lime, marl, inorganic fertilizers, and slurry (Pedersen 1995; Schjonning et al. 1994; Westh 1909), the expectation that grassland represents natural soil properties is highly uncertain. Archaeologically, relevant natural, undisturbed soils appear to be extremely rare in Denmark outside protected heathlands and ancient woodlands (Kristiansen and Dalsgaard 2000; Nielsen et al. 2019; Thomsen and Andreassen 2019), and no heathlands nor ancient woodlands are found on comparable parent materials surrounding Ribe.

Geostatistical analyses

In order to compare how different data sampling densities affect the spatial elemental patterns, two new grids were created based on the original 0.25-m × 0.25-m sample grid, creating in total three grids: 0.25 m × 0.25 m, 0.5 m × 0.5 m, and 1.0 m × 1.0 m (hereafter denoted 0.25-m, 0.5-m, and 1.0-m grid, respectively). For each grid size, each element (CaO, Cu, P₂O₅, and Sr) was analysed on its own. Descriptive statistics of elemental data constituting the three different grid resolutions are shown in Table 2. No transformation was applied to the data prior to kriging, and the individual data points were computed as the arithmetic mean of the three measurements per sample.

The spatial analyses were conducted using ordinary kriging in the software program “R” version 3.4.3 with the following add-on packages: sp, gstat, and raster; see Pebesma (2004, 2014) for details on kriging using the gstat package in R. A key part of the kriging procedure is the estimation of the so-called semivariogram. In the R-package, modelling of the different parameters (model, sill, range, and nugget) is allowed when fitting the semivariogram model. In turn, the semivariogram model is used for calculating the predicted (kriged) elemental concentrations, which are then shown as surface covering maps of the different elements as the output. Each map of predicted elemental concentrations is accompanied by a map of the standard deviation (% points) of the predicted values (weight %).

The semivariogram describes half of the mean variance between all possible point-pairs in the dataset as a function of distance or lag. The semivariogram values, γ , for the sampled parameter z are calculated at regular lags, h , as described below (Pebesma 2014):

$$\gamma(h) = \frac{1}{2N} \sum_{i=1}^N [z_i - z_{i+h}]^2 \quad (1)$$

where N is the number of pairs within the given lag interval, h ; z_i is the measurement of the regionalized variable taken at location i ; and z_{i+h} is another measurement taken h lag intervals away.

Table 2 Descriptive statistics of elemental data (%) for all three grid resolutions

Element	No. of samples	Min	Max	Mean	Standard deviation
CaO (0.25 m)	1059	0.742	12.984	3.593	1.270
Cu (0.25 m)	1059	0.002	1.116	0.042	0.068
P ₂ O ₅ (0.25 m)	1059	0.840	9.821	3.693	1.164
Sr (0.25 m)	1059	0.007	0.059	0.026	0.006
CaO (0.5 m)	277	0.835	10.711	3.549	1.308
Cu (0.5 m)	277	0.004	0.432	0.040	0.058
P ₂ O ₅ (0.5 m)	277	0.916	9.020	3.590	1.160
Sr (0.5 m)	277	0.011	0.059	0.025	0.006
CaO (1.0 m)	74	1.213	10.711	3.603	1.624
Cu (1.0 m)	74	0.005	0.325	0.035	0.054
P ₂ O ₅ (1.0 m)	74	1.081	9.018	3.618	1.365
Sr (1.0 m)	74	0.011	0.059	0.026	0.008

In order to obtain comparable results, modelling of the semivariogram parameters was based only on the 0.25-m grid dataset, since this sampling density contains spatial information starting from 0.25 m, but includes all the information on the 0.5 and the 1.0 sampling scale. Hence, for sampling distances over 1.0 m, the semivariograms should theoretically be the same and the observed differences arise because we have fewer data for the coarser grids and hence a more uncertain representation of the underlying true spatial statistics. The 0.25 fitted variogram model was therefore applied for the prediction maps of the 0.5-m and 1.0-m grids as well. The prediction grids for all cases are set at a 2-cm resolution to ensure that all relevant spatial details are captured.

We decided to fit the semivariogram model manually as opposed to automatic fitting with, for instance, a non-linear inversion. The rationale behind this is that it was prioritized to fit the first 2–3 data points (meaning up to a distance of 0.75 m) as well as possible, even though this might compromise the fitting for the data points on a larger distance. This approach was chosen because the semivariograms (Fig. 4) mainly display correlation up to around 1 m, while no or very little correlation exists between data points of a greater distance. Correlation between samples is a necessity for meaningful predictions of elemental concentrations in-between samples. The fitted semivariogram model parameters can be found in Table 3.

Results

Semivariograms

The semivariograms (Fig. 4) inform us about the spatial correlation of the measured data values in the grid points. The points are the experimental semivariance values and the solid line displays the fitted semivariogram model based on the 0.25-m grid points. When the experimental semivariances

are small, the data are strongly correlated at that distance and vice-versa for large semivariances. When the semivariogram flattens out, the correlation becomes smaller and approaches a value linked to the variance of the mean of all samples.

For three of the elements (CaO, P₂O₅, and Sr) and two of the grid resolutions (0.25 m and 0.5 m) (Fig. 4), the semivariograms show a steep slope up to a distance of 1–1.5 m. Hence, the CaO, P₂O₅, and Sr sample values are correlated within a 1–1.5-m distance from one another. Beyond 1.5 m, the elements lose their correlation. Thus, at a distance greater than 1–1.5 m, the sample points no longer provide useful information for the prediction of the elemental concentration.

The semivariograms (CaO, P₂O₅, and Sr) for the lowest resolution grid (1.0 m) do not display the same degree of correlation between sample points as the two higher resolution grids (0.25 m and 0.5 m). This tendency is due to the resolution of the dataset—all correlated information lies within a distance of 1 m.

Prediction of elemental concentrations and their uncertainties

Figures 5, 6, and 7 show both the predicted elemental concentrations and the standard deviation on the predicted values for CaO, P₂O₅, and Sr respectively. In the following, we will evaluate and compare the results visually. In the highest resolution (0.25-m grid), all of the elements display a large degree

Table 3 Model parameters of the best semivariogram-fit for each element based on the 0.25-m × 0.25-m grid

Element	Sill	Model	Range	Nugget
CaO	1.56801	Spherical	1.25	0.5704163
Cu	0.006732696	Exponential	2	0.0007280126
P ₂ O ₅	1.419789	Exponential	0.7	0.3056974
Sr	4.133472e-05	Exponential	0.7	1.207976e-05

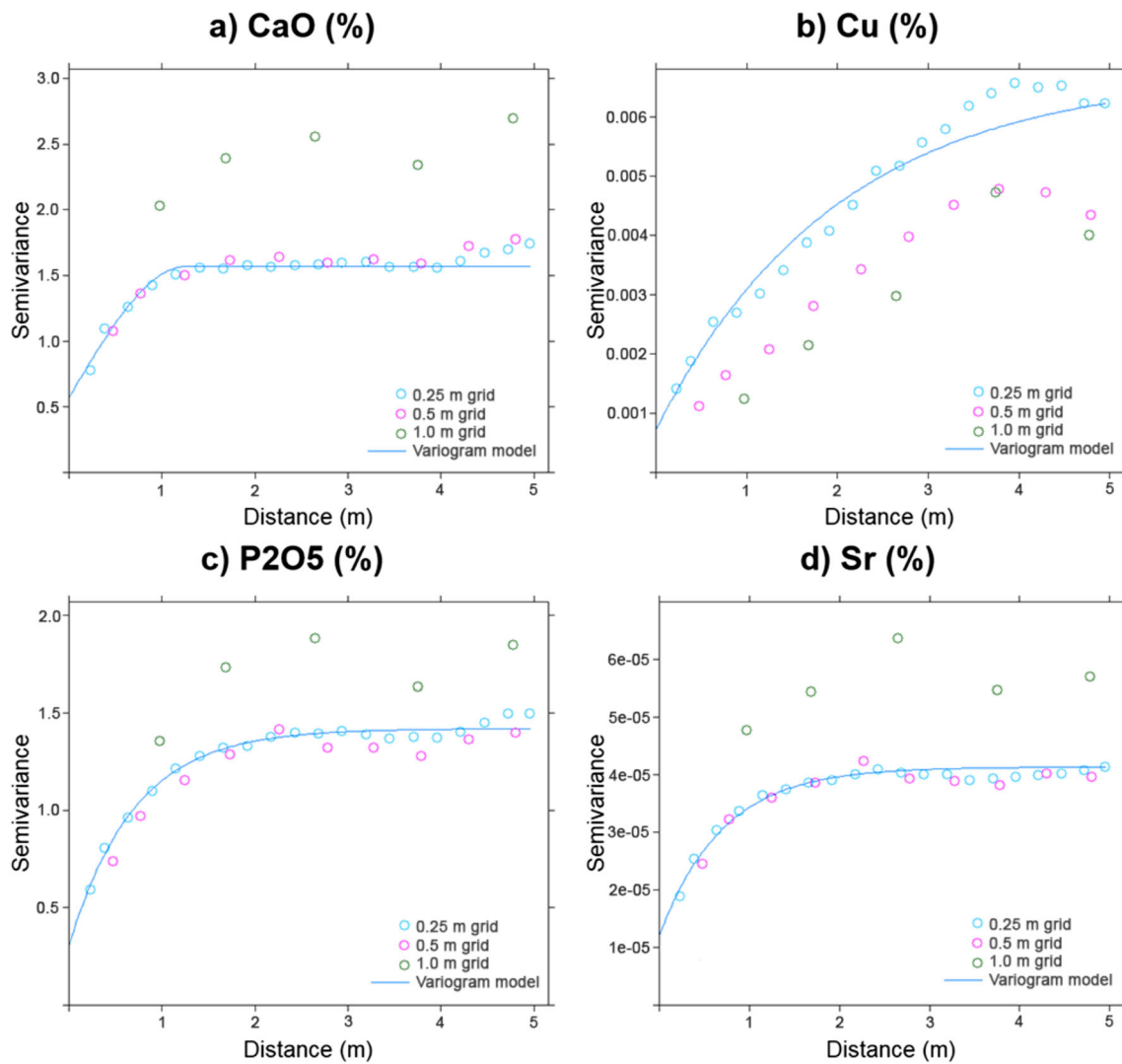


Fig. 4 Semivariograms showing the spatial correlation for CaO, Cu, P₂O₅, and Sr in the three grid resolutions (respectively 0.25 m × 0.25 m, 0.5 m × 0.5 m, and 1.0 m × 1.0 m) and the fitted models

of detail in the behaviour of the elements across the surface. The borders between high and low concentrations are also very clear; hence, the precise position and spreading of bounded concentration zones are easily recognized in the graphics. The 0.25-m grid resolution also displays low standard deviations between data points across the entire surface for CaO, P₂O₅, and Sr. The low standard deviation of the predicted concentrations indicates that this resolution is very well suited for prediction of precise elemental concentrations and, thus, a precise indication of the location of different possible indoor activity areas.

For the 0.5-m grid, the predicted elemental concentrations still show the location of areas with high and low concentrations relatively precisely, but the smaller areas are lost and the signal is more unclear. For the 0.5-m grid resolution, the standard deviations of the predicted elemental concentrations become larger than for the highest resolution; thus, the predicted maps are somewhat less accurate.

When the lowest resolution (1.0-m grid) is compared to the highest resolution (0.25-m grid), it is clear that the low-resolution dataset only shows main trends in the prediction of the elemental concentrations. With the low resolution, the borders between high and low concentrations become more blurred and the indications of smaller (possible) activity areas are completely lost. This lower resolution prediction is also followed by larger standard deviations when moving away from the observation points, and, hence, predicted values far from an observation point are more uncertain than the ones predicted by the highest resolution data set (0.25 m). In addition, since the semivariances on the 1.0-m grid (Fig. 4) are larger, a semivariogram model fitted to the 1.0-m grid instead of the 0.25-m grid would yield even larger uncertainties on the predicted concentrations. As the semivariograms in Fig. 4 demonstrate, the data values do not display correlation at a distance beyond 1–1.5 m. This also shows that

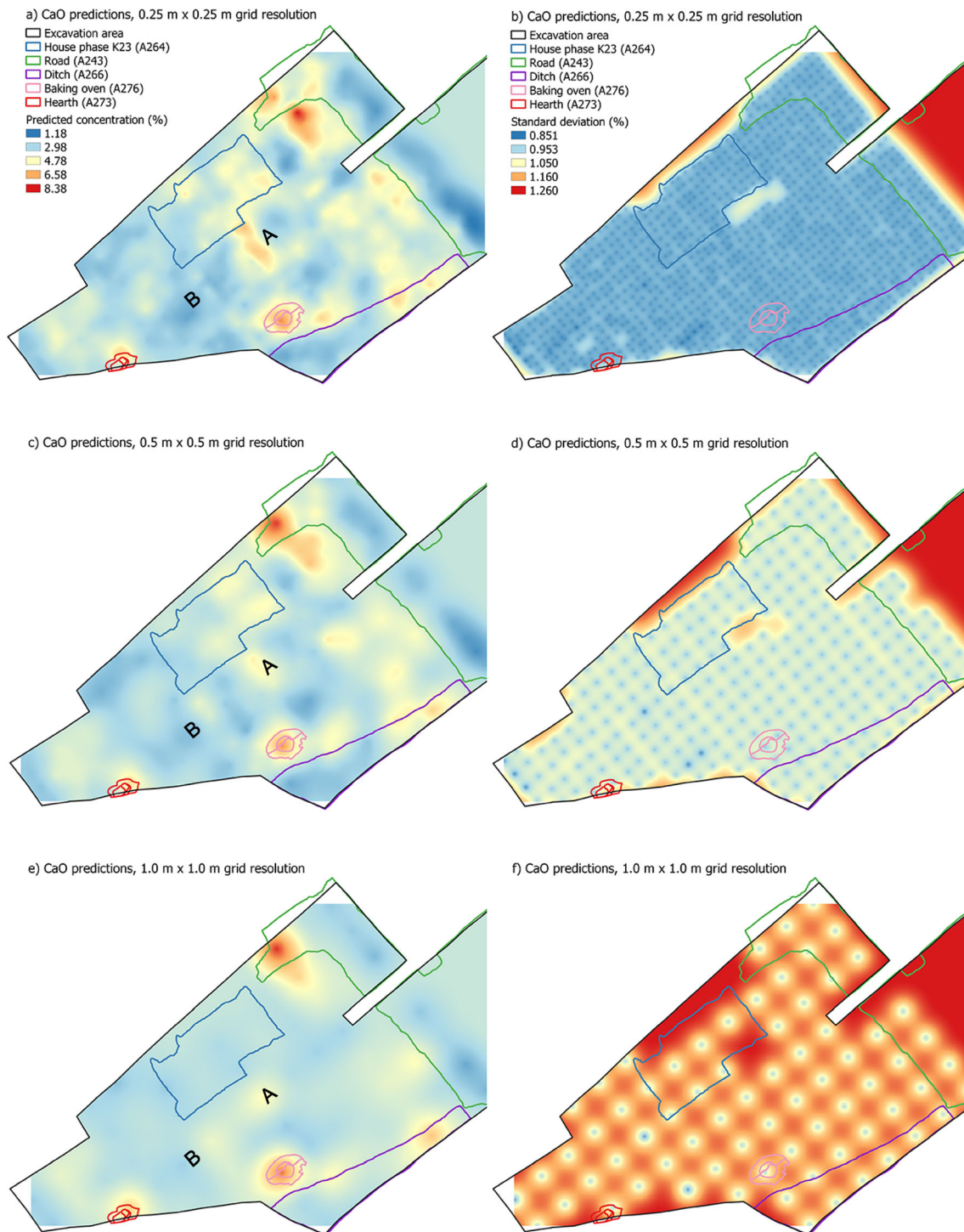


Fig. 5 Predicted surface elemental concentrations and variance on the predictions for CaO in the 0.25-m \times 0.25-m grid (a and b), 0.5-m \times 0.5-m grid (c and d), and 1.0-m \times 1.0-m grid (e and f)

the low-resolution data do not produce reliable prediction maps since the data points are on the outer limit of information about the neighboring data points. Another observation is that because the semivariograms indicate roughly the same spatial correlation lengths across the different elements, the uncertainty maps on the predictions are very

similar. If, for example, one of the semivariograms had been flatter with smaller values (i.e. less spatial variation), the uncertainty maps would have revealed smaller uncertainties moving away from an observation point.

Two features, “A” and “B”, are marked in Figs. 5, 6, and 7, showing potential activity zones not recognized



Fig. 6 Predicted surface elemental concentrations and variance on the predictions for P_2O_5 in the 0.25-m \times 0.25-m grid (a and b), 0.5-m \times 0.5-m grid (c and d), and 1.0-m \times 1.0-m grid (e and f)

during excavation. Feature A is an area of approximately 1.5 \times 0.5 m crossing the central aisle with elevated elemental concentrations. With the high resolution (0.25 m), this feature is very distinct in all predicted maps of CaO, P_2O_5 , and Sr. When the resolution is decreased to the 0.5-m grid, the feature becomes less evident and with the

lowest (1.0 m) resolution, it is no longer possible to recognize this area as an independent and possible activity zone. Feature B encompasses an area with depleted concentrations of all three elements stretching approximately 3 \times 1.5 m along the central aisle. Feature B is most prominent for P_2O_5 and Sr, while it is somewhat less clear in



Fig. 7 Predicted surface elemental concentrations and variance on the predictions for Sr in the 0.25-m × 0.25-m grid (a and b), 0.5-m × 0.5-m grid (c and d), and 1.0-m × 1.0-m grid (e and f)

the predictions of CaO. However, this seems to be due to the surrounding higher concentration areas, which are more pronounced for P₂O₅ and Sr, since concentrations of CaO are below the mean in this Feature. As was the case for Feature A, the high 0.25-m grid resolution clearly

demonstrates Feature B as different regarding the relative concentrations. When lowering the resolution, Feature B becomes less pronounced and with the 1.0-m grid, it is difficult to separate this as a distinct feature with depleted concentrations.

Hotspots

As described in “Introduction”, some elements might only reflect a few different activities, and, thus, can display a “hotspot tendency”. Here, this is the case for copper and as Fig. 8 shows, the distribution of high-concentration copper is restricted to the central part of the western side aisle belonging to house K23, marked as Feature “C”. Elsewhere, the concentration is very low, with only small copper accumulations spread across the eastern part of the house.

With the high-resolution dataset (0.25-m grid), the precise extent and concentration levels of Feature C can be discerned. It is clear that the distribution of the highest copper concentrations is very limited in extent, but that these are supported by high Cu-concentrations northeast of the hotspot. As the grid resolution is lowered (0.5-m grid), the hotspot area appears larger in extent and the very high copper concentrations in the centre of the hotspot are lost. The low-resolution 1.0-m grid only provides information about the area in which the hotspot is located, and not about its actual magnitude and extent. Additionally, the smaller copper accumulations outside of Feature C is no longer visible with the 1.0-m grid.

Discussion

How sampling density affects the outcome: field protocol and geostatistics

In archaeological research, the choice of interpolation grid density versus sampling density is a compromise especially based on the state of preservation of the deposits, and the excavation methods. The sampling density, sampling design, and geostatistics to interpolate the data are of paramount importance for the interpretation of mapping of any soil property, and we do not know *a priori* if the distribution of an element represents activity patterns preserved *in situ* or is biased by complex depositional and post-depositional processes (Webster 2000). The increased availability of rapid, non-destructive, and simultaneous multi-element analyses of exposed surfaces in the field and on soil samples in the laboratory furthermore requires good sampling practice. In our case, the heterogeneity and error types involved in sampling and processing were minimized by (a) collecting small composite samples, (b) applying representative mass reduction, (c) non-contaminating crushing, and (d) unbiased mixing before subsampling, as required in good sampling of heterogeneous materials (Esbensen et al. 2010). In Ribe’s well-defined stratigraphy, a near ideal field sampling protocol was possible despite significant truncation and

bioturbation (see e.g. voids on Figs. 5, 6, 7, and 8). On even more strongly bioturbated sites, in other climate zones, or with more heavily disturbed stratigraphy, however, greater difficulties are expected in this first step of the representative sampling. Nevertheless, the sampling density resulting from our clearly defined stratigraphic contexts is very likely to be applicable in other anthropogenic and archaeological studies of indoor contexts.

The choice of kriging for interpolation can result in local anomalies being smoothed out, while another side effect is that the interpolated data can be below or above the original data point(s). However, in both cases, the kriged values will be the *most likely estimate* as the sampled values are inherently uncertain as indicated by the size of the nugget value. In the case of mapping indoor space, this is likely of little concern in non-enriched areas where values cluster very much around an expected average background value or larger hotspots; whereas in cases where only few samples are at the extremes, this type of effect may disturb our ability to detect very small hotspots. Hence, close inspection of both absolute map colours and their standard deviation scale (Figs. 5, 6, 7, and 8) has to be considered carefully. Adding inverse distance weighting maps may help circumvent some of these problems, but can give rise to other, more serious issues, such as the ‘bulls eye’ effect, where hot- and coldspots may seem over-represented.

Considering the elemental maps of CaO, P₂O₅, and Sr in our study, the semivariograms in Fig. 4 show that the spatial correlations level out between 1 and 1.5 m of sampling space. This implies that the small-scale variation reflected by especially calcium is similar to the most anthropogenically influenced element, phosphorus, below this sampling distance. The metal copper, likely reflecting metalworking, by contrast, does not have a flat correlation beyond the local maximum of 3–4 m (Fig. 4). This is likely due to the high degree of clustering of this element (Fig. 8) and the presence of a hotspot, i.e. the archaeological area of interest.

It is not *a priori* known what the indoor correlation of elements is like, and, thus, knowledge from geochemical studies based on outdoor areas, which have different origins and preservation conditions, cannot be used to make assumptions about the spatial resolution of anthropogenic elemental markers in indoor settings. This study has demonstrated that it is possible to determine even small-scale changes in the elemental concentrations at resolutions as high as 0.25 m in indoor areas.

The semivariogram and kriging approach gave us important information about (1) degrees of correlation and correlation distances through the semivariograms, which in itself can be of value for the overall interpretation of the elemental distribution; (2) predicted maps, which

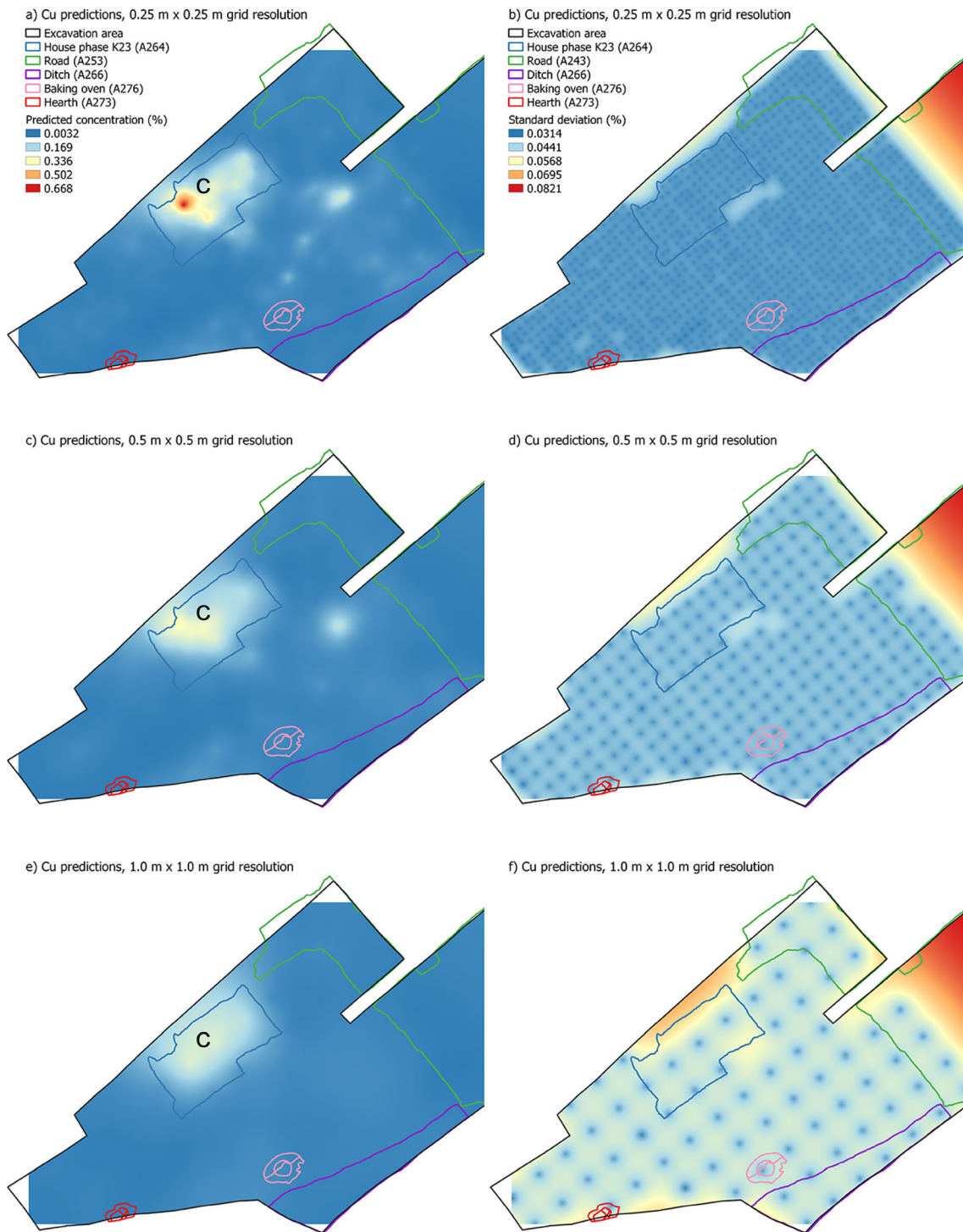


Fig. 8 Predicted surface elemental concentrations and variance on the predictions for Cu in the 0.25-m × 0.25-m grid (a and b), 0.5-m × 0.5-m grid (c and d), and 1.0-m × 1.0-m grid (e and f)

include information about the spatial variation of the actual data values incorporated in such a way that the maps can be thought of as the “most likely estimate” given the samples at hand; and (3) uncertainties associated with the predicted values, which in any given point

provide information about the degree to which the predicted value can be trusted. None of these items can be obtained with more traditional interpolation methods such as inverse distance, nearest neighbor or spline interpolation.

Archaeological implications: grid size choice

During excavation, it was established that there had been copper-alloy working in building K23. Based on the geochemical results, this metalwork is reflected in excavation unit A264 as revealed by the copper hotspot, also denoted as Feature C. Thus, here the geochemical data support the archaeological findings and provide additional knowledge about the spatial distribution and extent of these activities. On-site findings of both artefacts and recognition of differences in the deposits (i.e. colour or texture) do not always imitate the precise distribution and size of a given activity. This is demonstrated by the Cu distribution here, which shows the precise location where the metalworking was taking place and how large an area it covered. The results from this study show that it is crucial to apply high-density geochemical sampling to obtain a better understanding of the use of smaller spaces. Not only does the sampling density affect the detail in which we can resolve possible locations of rooms and the activities that have taken place there but it also determines which contexts can be recognized using geochemistry. Sampling with a low resolution (1.0-m grid) might not detect smaller areas such as hearths (e.g. excavation units A273 and A276 in Fig. 2c), which are reflected as higher concentrations of CaO, P₂O₅, and Sr (Figs. 5, 6, and 7), with more than one or two samples, which makes it impossible to determine if such geochemical readings are outliers (i.e. resulting from analysis or instrumental errors) or actual indications for archaeological activities. Unless the analysis is subject to a repeated error, outliers are not expected to cluster together in several samples, but rather be expressed as one or two erroneous readings. Some elements are related to only a couple of different activities, e.g. Cu, and to areas with special functions (Sulas et al. 2019). In such cases, they might display a hotspot tendency in indoor areas related to the activity. As also demonstrated by Feature A and B, representing possible activity areas of both enhanced and depleted concentrations, lowering the resolution removes the distinctness of such features. Feature A shows a narrow band of high concentrations of CaO, P₂O₅, and Sr crossing the central aisle and (possibly) linking the eastern and western side aisles. Since these three elements are all common anthropogenic markers (e.g. Mikołajczyk and Milek 2016; Milek and Roberts 2013; Sulas et al. 2017, 2019), an area with elevated concentrations with a suite of these elements might indicate intensive use of the area, as suggested by Cook et al. (2014). The band could then possibly indicate the preferred passageway between the two side aisles. In contrast to Feature A, Feature B shows an area with depleted elemental concentrations of all three common anthropogenic markers, especially visible in P₂O₅ and Sr. Areas with a general depletion of common elements could indicate that this was an area that was generally kept clean through e.g. sweeping (Fleisher and Sulas 2015), and hence preventing

accumulation. However, it has to be noted that interpretations should be based on a larger suite of elements than those included in this study, and other methods such as micromorphology to strengthen the interpretation.

Studies from Northwestern Europe (e.g. Abrahams et al. 2010; Mikołajczyk and Milek 2016) have shown that pXRF can be applied to distinguish activities in outdoor areas, such as on ancient farms and in coastal areas. However, previous studies of indoor space in Northwestern Europe have mainly comprised more costly multi-element methods such as ICP-AES (e.g. Milek and Roberts 2013; Wilson et al. 2008), and were conducted on a lower resolution scale of sampling. Applying quick and cost-efficient methods such as pXRF for the geochemical analysis offers the opportunity to include larger datasets and perform multiple measurements of each sample.

Smith et al. (2001) applied 0.25-m grid sampling for total phosphorus and magnetic susceptibility at the excavation of floors in Norse longhouses from Kilpheder in the Outer Hebrides. However, as in the case of others who chose to apply larger grid densities (e.g. Mikołajczyk and Milek 2016; Milek and Roberts 2013; Milek et al. 2014; Oonk et al. 2009; Sulas et al. 2019), the choice of sampling grid size or a specific rationale was not made explicit. As demonstrated in both the semivariograms and predicted elemental maps, the 0.25-m grid resolution displays very good correlation between sampling points and a very large degree of detail in the spatial element changes (e.g. as pointed out by Feature A, B and C in Figs. 5, 6, 7 and 8). However, since this high-resolution sampling also requires an extensive amount of time spent both on-site and in the laboratory compared to a 0.5-m grid, we recommend sampling in a 0.5-m grid for indoor spaces as a best-practice standard for developer-funded excavations. This is because the 0.5-m grid equally covers the correlation distances observed in the semivariograms, and still displays most of the details in the predicted maps. One could consider including higher resolution sampling, such as the 0.25-m grid, in specific (smaller) areas of interest, for instance if there are substantiated indications of geochemical hotspots based on on-site finds of artefacts, or on a larger scale where applicable, for example in the case of research excavations. Finally, if the variogram parameters are known beforehand, it is possible to optimize the sampling scheme to minimize sampling errors. However, this is rarely the case, and as a result, the application of spatial coverage schemes should be recommended because they rely only on the simple scattering of samples, as also pointed out by Wadoux et al. (2019).

With the results presented here, we hope to elucidate that the choice of sampling design should be carefully considered when excavating indoor spaces to obtain statistically reliable results from the geochemical record.

Conclusion

Applying fast and cost-efficient methods such as pXRF to the study of activity areas allows us to work on larger datasets and, thus, to increase the sampling resolution. This study demonstrates that a closer spacing between samples than commonly applied is needed for the samples to be spatially correlated to one another when studying indoor spaces, and hence for them to be useful for archaeological interpretations in developer-funded excavations.

The archaeological implications of the choice of sampling grid size, ranging from 0.25 m × 0.25 m to 1.0 m × 1.0 m, in this case illustrate the potential of increasing the sampling density to secure statistically well-founded elemental maps showing the detail in which we can resolve possible locations of past activities. Sampling using a high-density grid allows for better predictions of surface concentrations with reduced uncertainties on the predictions. High-resolution sampling also provides an opportunity for enhanced understanding of hotspots and coldspots, and enables the prediction of precise and smaller activity areas and the borders between them. The geochemical maps predicted in this study support archaeological findings such as the workshop for non-ferrous metalworking, but also add information about their spatial extent, which needs to be interpreted in conjunction with all archaeological evidence to fully make use of the potential of soil elemental mapping.

Based on the results of this study, we recommend as a best-practice standard for suspected archaeological indoor areas to sample on a grid with a maximum distance of 0.5 m between sample points, and preferably even smaller distances in the case of suspected areas of interest, or in the case of research excavations. As a result, it is possible to obtain statistically reliable measurements and predictions of element concentrations when examining activity horizons in indoor deposits.

Acknowledgements The authors would like to thank the entire excavation team working on the Northern Emporium excavation project. Special thanks to Thomas Ljungberg for significant guidance and help with the geostatistical data processing in R, and to the students who assisted with laboratory work. We would also like to thank Dr. Karen Milek for discussion and inputs in the early stage of this study. Finally, thank you to three anonymous reviewers who provided helpful comments and suggestions.

Funding The excavation and the Northern Emporium Project were funded by a Semper Ardens grant from the Carlsberg Foundation. This work was supported by the Danish National Research Foundation under the grant DNRF119 - Centre of Excellence for Urban Network Evolutions (UrbNet), and a postdoctoral research fellowship (12S7318N) of the Research Foundation Flanders – FWO.

Data availability The data that support the findings of this study are available on request from the corresponding author.

References

- Abrahams PW, Entwistle JA, Dodgshon RA (2010) The Ben Lawers historic landscape project: simultaneous multi-element analysis of former settlement and arable soils by X-ray fluorescence spectrometry. *J Archaeol Method Theory* 17:231–248. <https://doi.org/10.1007/s10816-010-9086-8>
- Barrett JH, Hall A, Johnstone C, Kenward H, & O'Connor T, Ashby S (2007) Interpreting the plant and animal remains from Viking-age Kaupang. In D. Skre (Ed.), *Kaupang in Skiringssal*. Kaupang Excavation Project Publication Series (Vol. 1, pp. 283–319). Aarhus University Press, Aarhus.
- Cannell RJS, Gustavsen L, Kristiansen M, Nau E (2018) Delineating an unmarked graveyard by high-resolution GPR and pXRF prospection: the Medieval Church Site of Furulund in Norway. *Comput Appl Archaeol* 1(1):1–18
- Cook SR, Clarke AS, Fulford MG (2005) Soil geochemistry and detection of early roman precious metal and copper alloy working at the roman town of Calleva Atrebatum (Silchester, Hampshire, UK). *J Archaeol Sci* 32(5):805–812
- Cook SR, Clarke AS, Fulford MG, Voss J (2014) Characterising the use of urban space: a geochemical case study from Calleva Atrebatum (Silchester, Hampshire, UK) Insula IX during the late first/early second century AD. *J Archaeol Sci* 50(1):108–116. <https://doi.org/10.1016/j.jas.2014.07.003>
- Crabtree PJ, Reilly E, Wouters B, Devos Y, Bellens T, Schryvers A (2017) Environmental evidence from early urban Antwerp: new data from archaeology, micromorphology, macrofauna and insect remains. *Quat Int* 460:108–123. <https://doi.org/10.1016/j.quaint.2017.08.059>
- Croix S (2015) Permanency in early medieval emporia: reassessing Ribe. *Eur J Archaeol* 18(3):497–523. <https://doi.org/10.1179/1461957114y.0000000078>
- Croix S, Deckers P, Feveile C, Knudsen M, Qvistgaard SS, Sindbæk SM, Wouters B (2019) Single context, metacontext, and high definition archaeology: integrating new standards of stratigraphic excavation and recording. *J Archaeol Method Theory* 26:1591–1631. <https://doi.org/10.1007/s10816-019-09417-x>
- Dalsgaard K (2005) Fygesandsaflejringer ved Ribe. In C. Feveile (Ed.), *Ribe Studier - Det ældste Ribe: Udgravninger på nordsiden af Ribe Å 1984-2000* (1.1, pp. 93–105). Jysk Arkæologisk Selskab/Den Antikvariske Samling.
- Dore CD, Varela SLL (2010) Kaleidoscopes, palimpsests, and clay: realities and complexities in human activities and soil chemical/residue analysis. *J Archaeol Method Theory* 17(3):279–302. <https://doi.org/10.1007/s10816-010-9092-x>
- Entwistle JA, McCaffrey KJW, Dodgshon RA (2007) Geostatistical and multi-elemental analysis of soils to interpret land-use history in the Hebrides, Scotland. *Geoarchaeology* 22(4):381–415. <https://doi.org/10.1002/geoa.20158>
- Esbensen KH, Guyot A, Westad F, Houmøller LP (2010) *Multivariate data analysis: in practice: an introduction to multivariate data analysis and experimental design*, 5th edn. Aalborg University
- Feveile C (2006) Ribe on the north side of the river, 8th–12th century—overview and Interpretation. In C. Feveile (Ed.), *Ribe Studier. Det Ældste Ribe. Udgravninger på nordsiden af Ribe Å 1984–2000*. Bind 1.1 (pp. 65–91). Jysk Arkæologisk Selskab.
- Feveile C (2010) Landskabet; Ribe opstår 700–865. In S. B. Christiansen (Ed.), *Ribe Bys Historie: 710–1520* (1st ed., pp. 20–38). Ribe, Dansk Center for Byhistorie.
- Feveile C (2012) Ribe: Emporia and town in 8th–9th century. In S. Gelichi & R. Hodges (Eds.), *From One Sea to Another. Trading Places in the European and Mediterranean Early Middle Ages*. Proceedings of the International Conference Comacchio, 27–29 March 2009 (pp. 111–122). Brepols Publishers.

- Feveile C, Jensen S (2000) Ribe in the 8th and 9th century: a contribution to the archaeological chronology of North Western Europe. *Acta Archaeologica* 71(1–2):9–24. <https://doi.org/10.1034/j.1600-0390.2000.d01-2.x>
- Fleisher J, Sulas F (2015) Deciphering public spaces in urban contexts: geophysical survey, multi-element soil analysis, and artifact distributions at the 15th–16th-century AD Swahili settlement of Songo Mnara, Tanzania. *J Archaeol Sci* 55:55–70. <https://doi.org/10.1016/j.jas.2014.12.020>
- Gé T, Courty M-A, Matthews W, Watzet J (1993) Sedimentary formation processes of occupation surfaces. In: Goldberg P, Nash DT, Petraglia MD (eds) *Formation Processes in Archaeological Context*. Prehistory Press, Madison (Wisconsin), pp 149–163
- Haslam R, Tibbett M (2004) Sampling and analyzing metals in soils for archaeological prospection: a critique. *Geoarchaeology* 19(8):731–751. <https://doi.org/10.1002/geo.20022>
- Horák J, Janovský M, Hejman M, Šmejda L, Klír T (2018) Soil geochemistry of medieval arable fields in Lovětín near Třešť, Czech Republic. *Catena* 162(April 2017):14–22. <https://doi.org/10.1016/j.catena.2017.11.014>
- Jensen S (1991) Dankirke - Ribe. Fra handelsgård til handelsplads. In: Mortensen P, Rasmussen BM (eds) *Fra stamme til stat i Danmark. 2: Høvdingsamfund og Kongemagt* (pp. 73–87) Jysk Arkæologisk Selskab
- Kristiansen SM, Dalsgaard K (2000) Soil evolution in the remnants of natural forest vegetation: an example from an old oak-lime coppice forest in Denmark. *Geografisk Tidsskrift* 100:27–37
- Linderholm J (2007) Soil chemical surveying: a path to a deeper understanding of prehistoric sites and societies in Sweden. *Geoarchaeology* 22(4):417–438. <https://doi.org/10.1002/geo.20159>
- Lubos C, Dreibrodt S, Bahr A (2016) Analysing spatio-temporal patterns of archaeological soils and sediments by comparing pXRF and different ICP-OES extraction methods. *J Archaeol Sci Rep* 9:44–53. <https://doi.org/10.1016/j.jasrep.2016.06.037>
- Macphail RI, Cruise GM, Allen MJ, Linderholm J, Reynolds P (2004) Archaeological soil and pollen analysis of experimental floor deposits; with special reference to Butser Ancient Farm, Hampshire, UK. *J Archaeol Sci* 31(2):175–191
- Macphail RI, Bill J, Crowther J, Haită, Constantin Linderholm J, Popovici D, Rødsrud CL (2016) European ancient settlements – a guide to their composition and morphology based on soil micromorphology and associated geoarchaeological techniques; introducing the contrasting sites of Chalcolithic Borđușani-Popină, Borcea River, Romania and Viking Age. *Quat Int* 460:30–47. <https://doi.org/10.1016/j.quaint.2016.08.049>
- Mertz EL (1977) Ribe og omegns jordbundsforhold: En ingeniørgeologisk beskrivelse (By-geologi). C.A. Reitzels Forlag.
- Mikolajczyk L, Milek K (2016) Geostatistical approach to spatial, multi-elemental dataset from an archaeological site in Vatnsfjörður, Iceland. *J Archaeol Sci Rep* 9:577–585. <https://doi.org/10.1016/j.jasrep.2016.08.036>
- Milek KB (2012) Floor formation processes and the interpretation of site activity areas: an ethnoarchaeological study of turf buildings at Thverá, northeast Iceland. *J Anthropol Archaeol* 31(2):119–137. <https://doi.org/10.1016/j.jaa.2011.11.001>
- Milek KB, Roberts HM (2013) Integrated geoarchaeological methods for the determination of site activity areas: a study of a Viking Age house in Reykjavik, Iceland. *J Archaeol Sci* 40(4):1845–1865. <https://doi.org/10.1016/j.jas.2012.10.031>
- Milek K, French C (2007) Soils and sediments in the settlement and harbour at Kaupang. In: Skre D (ed) *Kaupang in Skiringssal, Kaupang Excavation Project Publication Series*. Aarhus University Press, Aarhus, pp 321–360
- Milek K, Zori D, Connors C, Baier W, Baker K, & Byock J (2014) Interpreting social space and social status in the Viking Age house at Hrisbrú using integrated geoarchaeological and microfossil analyses. In D. Zori & J. Byock (Eds.), *Viking Archaeology in Iceland: The Mosfell Archaeological Project* (pp. 143–162). 10.1484/M.CURSORS-EB.1.102218
- Nicolodelli G, Cabral J, Menegatti CR, Marangoni B, Senesi GS (2019) Recent advances and future trends in LIBS applications to agricultural materials and their food derivatives: An overview of developments in the last decade (2010–2019). Part I. Soils and fertilizers. *TrAC - Trends Analyt Chem* 115:70–82
- Nielsen NH, Kristiansen SM, Ljungberg T, Enevold R, & Løvschal M (2019) Low and variable: manuring intensity in Danish Celtic fields. *Journal of Archaeological Science: Reports*, 27. <https://doi.org/10.1016/j.jasrep.2019.101955>
- O'Rourke SM, Minasny B, Holden NM, McBratney AB (2016) Synergistic Use of Vis-NIR, MIR, and XRF Spectroscopy for the determination of soil geochemistry. *Soil Sci Soc Am J* 80(4):888–899. <https://doi.org/10.2136/sssaj2015.10.0361>
- Oliver MA, Webster R (2014) A tutorial guide to geostatistics: computing and modelling variograms and kriging. *Catena* 113:56–69
- Oonk S, Slomp CP, Huisman DJ, Vriend SP (2009) Effects of site lithology on geochemical signatures of human occupation in archaeological house plans in the Netherlands. *J Archaeol Sci* 36(6):1215–1228. <https://doi.org/10.1016/j.jas.2009.01.010>
- Pebesma EJ (2004) Multivariable geostatistics in S: The gstat package. *Comput Geosci* 30(7):683–691. <https://doi.org/10.1016/j.cageo.2004.03.012>
- Pebesma EJ (2014) gstat user 's manual. Retrieved from Gstat user's manual 2.5.1 website: <http://www.gstat.org/>
- Pedersen JB (1995) *De danske Kalk- og Mergelselskaber: Kalk og mergel gennem tiderne*. De Danske Kalk- Og Mergelselskaber, Viborg, 95.
- Pîrnău RG, Patriche CV, Roșca B, Vasiliniuc I, Vornicu N, Stanc S (2020) Soil spatial patterns analysis at the ancient city of Ibida (Dobrogea, SE Romania), via portable X-ray fluorescence spectrometry and multivariate statistical methods. *Catena* 189(February):1–12. <https://doi.org/10.1016/j.catena.2020.104506>
- Reimann C, Fabian K, Birke M, Filzmoser P, Demetriades A, Négrel P, Oorts K, Matschullat J, Caritat P, The GEMAS Project Team (2018) GEMAS: establishing geochemical background and threshold for 53 chemical elements in European agricultural soil. *Appl Geochem* 88:302–318
- Rondelli B, Lancelotti C, Madella M, Pecci A, Balbo A, Pérez JR, Inserra F, Gadekar C, Ontiveros MAC, Ajithprasad P (2014) Anthropogenic activity markers and spatial variability: an ethnoarchaeological experiment in a domestic unit of Northern Gujarat (India). *J Archaeol Sci* 41:482–492. <https://doi.org/10.1016/j.jas.2013.09.008>
- Save S, Kovacic J, Demarly-Cresp F, Isenmann R, Poirier S, Sedlbauer S, Teyssonneyre Y (2020) Large-scale geochemical survey by pXRF spectrometry of archaeological settlements and features: new perspectives on the method. *Archaeol Prospect* 27:1–16. <https://doi.org/10.1002/arp.1773>
- Schjonning P, Christensen BT, Carstensen B (1994) Physical and chemical-properties of a sandy loam receiving animal manure, mineral fertilizer or no fertilizer for 90 years. *Eur J Soil Sci* 45(3):257–268
- Sindbæk SM (2018) Northern Emporium: the archaeology of urban networks in Viking Age Ribe. In R. & S. S. Raja (Eds.), *Urban Network Evolutions. Towards a high-definition archaeology* (pp. 161–166). Aarhus, Aarhus University Press.
- Skre Dagfinn. (2007). *Kaupang in Skiringssal. Kaupang Excavation Project Publication Series* (1. Norske). Aarhus University Press.
- Šmejda L, Hejman M, Horák J, Shai I (2018) Multi-element mapping of anthropogenically modified soils and sediments at the Bronze to Iron Ages site of Tel Burna in the southern Levant. *Quat Int* 483: 111–123. <https://doi.org/10.1016/j.quaint.2017.11.005>
- Smith H, Marshall P, Pearson MP (2001) Reconstructing house activity areas. In U. Albarella (Ed.), *Environmental Archaeology: Meaning*

- and Purpose (pp. 249–270). <https://doi.org/10.1007/978-94-015-9652-7>
- Stockmann U, Cattle SR, Minasny B, McBratney AB (2016) Utilizing portable X-ray fluorescence spectrometry for in-field investigation of pedogenesis. *Catena* 139:220–231. <https://doi.org/10.1016/j.catena.2016.01.007>
- Sulas F, Fleisher J, Wynne-Jones S (2017) Geoarchaeology of urban space in tropical island environments: Songo Mnara, Tanzania. *J Archaeol Sci* 77:52–63. <https://doi.org/10.1016/j.jas.2016.06.002>
- Sulas F, Kristiansen SM, Wynne-Jones S (2019) Soil geochemistry, phytoliths and artefacts from an early Swahili daub house, Unguja Ukuu, Zanzibar. *J Archaeol Sci* 103(May 2018):32–45. <https://doi.org/10.1016/j.jas.2019.01.010>
- Thompson AE, Meredith CR, Prufer KM (2018) Comparing geostatistical analyses for the identification of neighborhoods, districts, and social communities in archaeological contexts: a case study from two ancient Maya centers in southern Belize. *J Archaeol Sci* 97(June):1–13. <https://doi.org/10.1016/j.jas.2018.06.012>
- Thomsen E, Andreasen R (2019) Agricultural lime disturbs natural strontium isotope variations: implications for provenance and migration studies. *Sci Adv* (3):5, eaav8083
- Wadoux AMJ, Marchant BP, Lark RM (2019) Efficient sampling for geostatistical surveys. *Eur J Soil Sci* 70:975–989. <https://doi.org/10.1111/ejss.12797>
- Webster R (2000) Is soil variation random? *Geoderma* 97:149–163. [https://doi.org/10.1016/S0016-7061\(00\)00036-7](https://doi.org/10.1016/S0016-7061(00)00036-7)
- Webster R, Oliver MA (1990) *Statistical methods in soil and land resource survey*. Oxford University Press
- Wells EC, Novotny C, Hawken JR (2007) Predictive modeling of soil chemical data by ICP-OES reveals the uses of ancient Mesoamerican plazas. In: Glascock MD, Speakman RJ, Popelka-Filcoff RS (eds) *Archaeological chemistry: Analytical techniques and archaeological interpretation*. American Chemical Society, Washington, DC, pp 210–230
- Wells EC (2010) Sampling design and inferential bias in archaeological soil chemistry. *J Archaeol Method Theory* 17:209–230. <https://doi.org/10.1007/s10816-010-9087-7>
- Westh TC (1909) Eng og mose, mergel. In: Jacobsen A (ed) *Hedebogen - korte populære bidrag om heden i fortiden, nutiden og fremtiden* (pp. 72–79) København
- Wilson CA, Davidson DA, Cresser MS (2005) An evaluation of multi-element analysis of historic soil contamination to differentiate space use and former function in and around abandoned farms. *The Holocene* 15(7):1094–1099. <https://doi.org/10.1191/0959683605h1881r>
- Wilson CA, Davidson DA, Cresser MS (2008) Multi-element soil analysis: an assessment of its potential as an aid to archaeological interpretation. *J Archaeol Sci* 35:412–424. <https://doi.org/10.1016/j.jas.2007.04.006>
- Woodruff LG, Cannon WF, Eberl DD, Smith DB, Kilburn JE, Horton JD, Garrett RG, Klassen RA (2009) Continental-scale patterns in soil geochemistry and mineralogy: results from two transects across the United States and Canada. *Appl Geochem* 24(8):1369–1381. <https://doi.org/10.1016/j.apgeochem.2009.04.009>
- Zhao C, Zhang Y, Wang CC, Hou M, Li A (2019) Recent progress in instrumental techniques for architectural heritage materials. *Herit Sci* 7(1):7–36

Publisher's note Springer Nature remains neutral with regard to jurisdictional claims in published maps and institutional affiliations.